

A DEBRIS DISK AROUND THE CENTRAL STAR OF THE HELIX NEBULA?

K. Y. L. SU,¹ Y.-H. CHU,² G. H. RIEKE,¹ P. J. HUGGINS,³ R. GRUENDL,² R. NAPIWOTZKI,⁴
 T. RAUCH,⁵ W. B. LATTER,⁶ AND K. VOLK⁷

Received 2006 December 22; accepted 2007 January 22; published 2007 February 13

ABSTRACT

Excess emission from a pointlike source coincident with the central star of the Helix Nebula is detected with *Spitzer* at 8, 24, and 70 μm . At 24 μm , the central source is superposed on an extended diffuse emission region. While the [O IV] 25.89 μm line contributes to the diffuse emission, a 10–35 μm spectrum of the central source shows a strong thermal continuum. The excess emission from the star most likely originates from a dust disk with blackbody temperatures of 90–130 K. Assuming a simple optically thin debris disk model, the dust is distributed in a ring between ~ 35 and ~ 150 AU from the central star, possibly arising from collisions of Kuiper Belt–like objects or the breakup of comets from an Oort-like cloud that have survived from the post–main–sequence evolution of the central star.

Subject headings: infrared: stars — stars: individual (WD 2226–210) — white dwarfs

Online material: color figures

1. INTRODUCTION

The Helix Nebula (NGC 7293), at only 219 pc (Harris et al. 2007), is one of the best-studied planetary nebulae. *Hubble Space Telescope* (*HST*) images at optical wavelengths and recent *Spitzer Space Telescope* (*Spitzer*) images at 3.6–8 μm have resolved the Helix Nebula into thousands of “cometary knots” immersed in diffuse gas, producing strikingly beautiful and well-publicized images (O’Dell et al. 2004; Hora et al. 2006). In contrast, *Chandra* X-ray observations of the Helix detected only a point source associated with the central star, but the X-ray properties of this source are mysterious.

The central star of the Helix Nebula, WD 2226–210, is a $\sim 110,000$ K hot white dwarf (Napiwotzki 1999; Traulsen et al. 2005). As expected, its photosphere emits soft X-rays at energies up to ~ 0.25 keV; however, *Chandra* and *Röntgensatellit* observations revealed additional hard X-ray emission near 1 keV (Leahy et al. 1994; Guerrero et al. 2001). The luminosity, temporal variations, and spectral properties of this hard X-ray component (Guerrero et al. 2001) and the variability of WD 2226–210’s H α emission-line profile (Gruendl et al. 2001) are consistent with the coronal activity of an M dwarf. However, a sensitive *HST* search has ruled out the presence of any companion with a spectral type earlier than M5 (Ciardullo et al. 1999).

The mystery regarding the central star of the Helix Nebula deepens with new *Spitzer* observations at 24 and 70 μm , as reported in this Letter.

2. OBSERVATIONS, DATA REDUCTION, AND ANALYSIS

The Helix Nebula was observed with all three *Spitzer* instruments: the Infrared Array Camera (IRAC; Fazio et al. 2004), the Infrared Spectrograph (IRS; Houck et al. 2004), and the Mul-

tiband Imaging Photometer for *Spitzer* (MIPS; Rieke et al. 2004). The MIPS observations were made in the scan map mode with a medium scan rate and a half-array offset, resulting in an effective integration of 80 s per pointing and covering an area of $0.5^\circ \times 0.8^\circ$ in each of the 24, 70, and 160 μm bands. Three MIPS scan maps were taken in sequence with ≥ 10 hr separations to avoid confusion by asteroids. The IRS high-resolution observations of the central star and a nearby nebular position were made in sequence in the staring mode. The IRAC observations have been described in detail by Hora et al. (2006).

Basic reduction for the MIPS data was carried out using the MIPS Data Analysis Tool (Gordon et al. 2005). IRAC mosaics were generated from the *Spitzer* Science Center (SSC) Basic Calibrated Data (BCD) product (ver. S13.2) using a customized IDL program. The central $15.4' \times 12.5'$ region of the nebula at 3.6, 4.5, 8.0, 24, 70, and 160 μm is displayed in Figure 1 (Plate 1). IRS high-resolution spectra were extracted from the SSC BCD product (ver. S14.0) using the IRS team’s Spectral Modeling, Analysis, and Reduction Tool (SMART; Higdon et al. 2004). As the spectra on the star were extracted using a full-slit width mode in both the Short-High (SH, 9.9–19.6 μm , $5'' \times 11''$ slit) and Long-High (LH, 18.7–37.2 μm , $11'' \times 22''$ slit) modules without off-source sky subtraction, the LH spectrum was scaled to match the continuum level of the SH spectrum. The scaled LH spectrum and the SH spectrum are plotted together in the top panel of Figure 2.

The IRAC images of the Helix Nebula show a bare point source at the location of the central star, WD 2226–210 (see Fig. 1). This central source is detected with flux densities of 374 ± 19 , 241 ± 24 , 171 ± 26 , and 174 ± 17 μJy at the 3.6, 4.5, 5.8, and 8.0 μm IRAC bands, respectively. The flux densities in the first three bands are, within error limits, consistent with those expected from the Rayleigh-Jeans tail of a 110,000 K blackbody model normalized to the Two Micron All Sky Survey (2MASS) photometry of the star (2MASS 22293854–2050136), $J = 14.332 \pm 0.024$, $H = 14.490 \pm 0.039$, and $K_s = 14.548 \pm 0.079$. The flux density at 8 μm is, however, twice as high as expected.

The MIPS images of the Helix Nebula show very different distributions of emission. In the 24 μm band, a pointlike source coincident with the central star is superposed on a plateau of diffuse emission. In the 70 μm band, no diffuse emission is seen,

¹ Steward Observatory, University of Arizona, Tucson, AZ; ksu@as.arizona.edu.

² Department of Astronomy, University of Illinois at Urbana-Champaign, Urbana, IL.

³ Physics Department, New York University, New York, NY.

⁴ Centre for Astrophysics Research, Science and Technology Research Institute, University of Hertfordshire, Hatfield, UK.

⁵ Institut für Astronomie und Astrophysik, Universität Tübingen, Tübingen, Germany.

⁶ NASA *Herschel* Science Center, California Institute of Technology, Pasadena, CA.

⁷ Gemini Observatory, Hilo, HI.

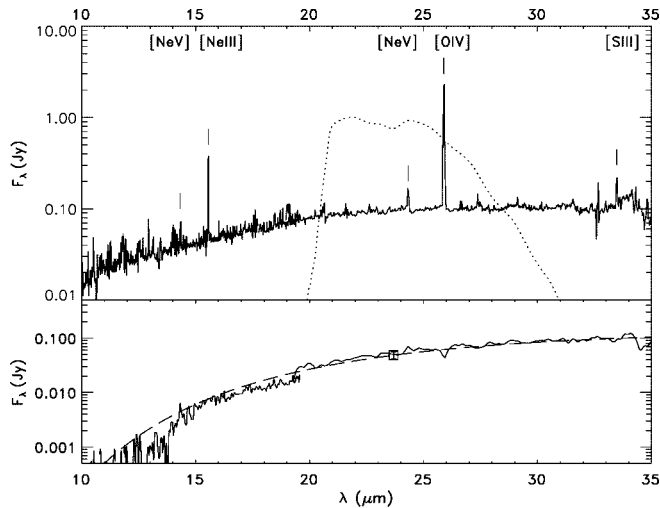


FIG. 2.—*Spitzer* spectrum of the Helix central star. The top panel shows the spectrum without sky (nebula) subtraction; therefore, the spectrum contains contributions from nebula, zodiacal background, and the central point source. For comparison, the MIPS 24 μm bandpass is shown as a dotted line in the top panel. The bottom panel shows the spectrum from the central source after nebular and sky subtraction and Gaussian smoothing (with no scaling between SH and LH modules). MIPS 24 μm photometry is shown as a square. A blackbody of 102 K is superposed as a long dashed line. [See the electronic edition of the *Journal* for a color version of this figure.]

and only a central pointlike source is detected. In the 160 μm band, neither the central source nor the bright diffuse emission is detected.

To analyze the central pointlike source at 24 μm , the bright diffuse background needs to be subtracted. The surface brightness of the diffuse emission falls off linearly with radius (r) from the central star. Therefore, we use a linear model fit to the surface brightness profile between $r = 31''$ and $100''$ to estimate the diffuse emission superposed on the central pointlike source. After background subtraction, the central source appears slightly resolved with a FWHM of $\sim 9''$, 1.5 times that of a true point source, possibly due to an imperfect subtraction of the background. Using aperture photometry and a color correction for a ~ 100 K blackbody (see § 3.3 for justification), the background-subtracted flux density of the central source is 48.4 ± 7.3 mJy in the 24 μm band. No variability is detected at 24 μm in our three observations. Using a similar method, we measure a flux density of 224 ± 33 mJy in the 70 μm band and a 3σ upper limit of 237 mJy in the 160 μm band.

3. DISCUSSION

3.1. The Diffuse Emission and Point-Source Regions

The detection of a pointlike source in the MIPS 24 and 70 μm bands is puzzling because the large extent of the ionized nebula is well resolved with *Spitzer*. While the MIPS 24 μm flux from the unresolved source could originate from emission lines in the bandpass, the lines would have to originate in high-ionization stages from abundant elements. Possible lines are the [Ne v] 24.32 μm line and [O iv] 25.89 μm line, the latter having been suggested by Leene & Pottasch (1987) from the *IRAS* observation. The ionization thresholds needed to produce O iv (54.9 eV) and to excite the $\lambda 4686$ line by the ionization and recombination of He ii (54.4 eV) are similar. Therefore, we resort to a He ii $\lambda 4686$ image of the Helix Nebula (O'Dell et al. 2004) to assess the spatial extent of the [O iv] emission at a higher resolution. The He ii image of the Helix Nebula

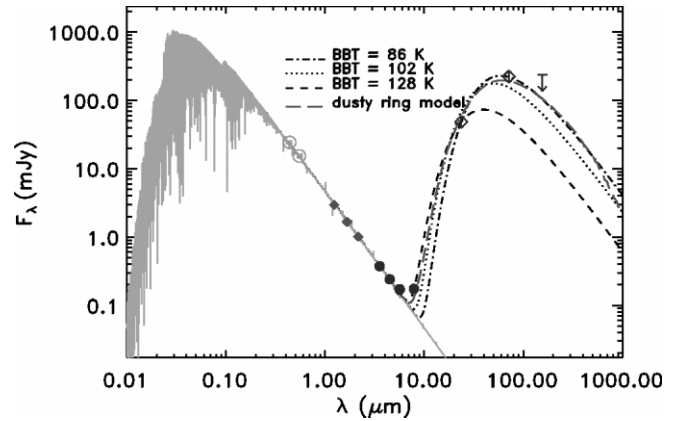


FIG. 3.—SED of the central white dwarf in the Helix Nebula. The photometry for ground-based Johnson *B* and *V* (Harris et al. 2007) is displayed as open circles, as filled diamonds for 2MASS, filled circles for IRAC, and open diamonds for MIPS photometry with a downward arrow showing the 160 μm 3σ upper limit. The white dwarf photospheric model is shown as a gray line. The excess SED is consistent with a blackbody with temperatures (BBT) ranging from 86 K (the best fit using MIPS 24 and 70 μm points) to 128 K (the best fit using IRAC 8 μm and MIPS 24 μm). An intermediate temperature of 102 K is also shown as a heavy dotted line for comparison. The SED of a dusty ring (35–150 AU) is shown as a long-dashed line. [See the electronic edition of the *Journal* for a color version of this figure.]

shows a central diffuse emission region similar to that seen at 24 μm , but not a pointlike central source. From this comparison we conclude that the [O iv] line contributes to the diffuse emission up to a radius of $\sim 2'$.

The absence of the central pointlike source in the He ii image confirms that the [O iv] line does not contribute to the central peak in the MIPS 24 μm band. Another promising candidate is the [Ne v] 24.32 μm line. With an excitation potential of 97 eV, Ne v can be produced via photoionization by hard X-rays or thermal collisional ionization at temperatures (T) higher than 10^5 K. At such high temperatures, the He ii $\lambda 4686$ recombination line may be weakened to below the detection limit because of its $T^{-1/2}$ dependence. While this might explain the absence of the central peak in the He ii image, it cannot explain the central pointlike source in the MIPS 70 μm band, as this band does not contain any nebular lines of abundant elements at high-ionization stages.

Both [O iv] and [Ne v] lines are seen in our IRS spectrum of the central region (see the top panel of Fig. 2) on top of a continuum (a combination of dust grains in the ionized nebula, zodiacal background and the central point source). Without a proper subtraction of the nebular and zodiacal contribution, it is difficult to assess the relative importance of the emission lines and the continuum from the central star based on this IRS spectrum alone. The true spectrum of the central source is revealed after subtraction of the nebular and sky contribution (shown in the bottom panel of Fig. 2). The spectrum of the central source will be addressed in more detail in another paper.

3.2. Nature of the Central Infrared Source

The spectral energy distribution (SED) of the central source is shown in Figure 3. For the white dwarf, we employ TMAP, the Tübingen NLTE Model Atmosphere Package (Werner et al. 2003; Rauch & Deetjen 2003), in its most recent version for the calculation of plane-parallel, static white dwarf models that consider H–He–C–N–O–Mg–Si–Ca–Ni model atoms. The SED shortward of 6 μm is consistent with the scaled white dwarf photospheric model for 110,000 K. Assuming that the excess

infrared emission originates from a blackbody radiator, its temperature is 90–130 K (see Fig. 3), far too low for a stellar object. If the blackbody radiator is heated by the central star WD 2226–210, of which the effective temperature is 110,000 K and radius is $0.024 R_{\odot}$, it would have to be 41–91 AU from the star. This radial distance corresponds to $0.19''$ – $0.42''$, so it cannot be resolved with *Spitzer*. The luminosity of this blackbody radiator, $(5.1\text{--}11) \times 10^{31}$ ergs s^{-1} , requires a total cross section (σ_{tot}) of $(0.8\text{--}8.7) \times 10^{27}$ cm 2 , or 3.8–38 AU 2 . Although we do not have any constraint on the geometry of the emission source, only an extended dust cloud, most probably a disk can provide such a large emitting area. The extinction toward the star is small based on the *International Ultraviolet Explorer* data (Bohlin et al. 1982), consistent with the 219 pc distance. The dust disk is likely to be optically thin and tilted since the main nebular ring is tilted by $\sim 35^\circ$ with respect to the line of sight (Young et al. 1999).

Given the evolution of the Helix central star through the asymptotic giant branch (AGB) and planetary nebula phases, the presence of a debris disk from the stellar main-sequence phase is surprising but not entirely impossible. Recently, dust disks around the white dwarf GD 362 (Becklin et al. 2005; Kilic et al. 2005) and the white dwarf G29-38 (Zuckerman & Becklin 1987; Reach et al. 2005) were reported; these disks are closer to their central stars and thus have SEDs showing excess emission starting from the near-IR bands. The Helix central star is much hotter and more luminous than these two white dwarfs (i.e., the Helix central star is much less evolved along its cooling track than the other two); thus, it can heat a debris disk at a larger radial distance.

3.3. Physical Properties of the Debris Disk

If the infrared excess around the Helix central star indeed arises from a debris disk, the dust grains in the disk that dominate the radiation are likely to be microns to millimeters in size. The minimum grain size will be set by blowout by radiation pressure. Given the stellar mass of $0.58 M_{\odot}$ (Napiwotzki 1999; Traulsen et al. 2005) and a luminosity of $76 L_{\odot}$ (from the observed photometry and distance), grains smaller than $\sim 60 \mu\text{m}$ will be ejected from the system. For an initial estimate, one can assume that the disk consists of grains with sizes (radius of a) from 60 to 1000 μm and has a power-law size distribution, $n(a) \propto a^{-3.5}$, as expected for a collision-dominated disk (Dohnanyi 1969; Tanaka et al. 1996). The relatively large grains support using blackbody-based approximations to characterize the system.

For a simple estimate, we take the disk dimensions from the preceding section and approximates the grain size distribution by a single size of 100 μm , characteristic of the grains that dominate the infrared emission. The dust mass in these grains is $(4/3) \rho_g a \sigma_{\text{tot}}$ where ρ_g is the grain density and σ_{tot} is the total area that intercepts the star light. Since the total dust mass is proportional to $\int n(a) a^3 da \propto a^{0.5}$, the total dust mass from the disk is $\sim 0.11 M_{\oplus}$ assuming $\rho_g = 2.5 \text{ g cm}^{-3}$ and $\sigma_{\text{tot}} = 6 \times 10^{27} \text{ cm}^2$.

This rough estimate can be tested with a more realistic model that fits the SED, although such models are still subject to degeneracy and ambiguities. We assume that the grains are astronomical silicates (Laor & Draine 1993) with a size distribution as before. The disk is optically thin, is heated only by WD 2226–210, and has a constant surface number density, with inner and outer boundaries of r_{in} and r_{out} . The observed SED is fitted by a ring extending from 35 to 150 AU with a total dust mass of $0.13 M_{\oplus}$ ($\pm 50\%$), as shown in Figure 3.

The exact inner radius of the disk is subject to the grain

properties used in the model; however, the inner radius cannot be too close to the star because no observable excess is found at wavelengths shorter than 8 μm . An inner hole is required from the SED modeling. The outer boundary of the disk is constrained in our model because a disk with a much larger outer radius would have higher 160 μm flux, contradicting the observed upper limit. Therefore, the dust around the Helix central star is in a form of ring between ~ 35 and ~ 150 AU. This configuration is remarkably similar to the planetary debris disks seen around main-sequence stars.

3.4. Origin of the Debris Disk

What is the origin of the dust *Spitzer* detects around the Helix central star? It has been established that any planet closer than ~ 1 AU will be engulfed by an expanding red giant (Siess & Livio 1999a, 1999b), while planets outside ~ 5 AU from the Sun will survive post-main-sequence evolution (Sackmann et al. 1993; Debes & Sigurdsson 2002), and the orbits of surviving planets and most of the Kuiper Belt objects (KBOs) and Oort Cloud comets will expand adiabatically and remain bound to the solar system (Duncan & Lissauer 1998). The restabilized KBOs and Oort Cloud can later become the source of objects that go into the inner part of the system, either plunging into the white dwarf or breaking up due to tidal destruction, and they can populate the inner system with dust. A similar scenario has been proposed to explain the photospheric metal contamination in DAZ white dwarfs (Stern et al. 1990; Parriott & Alcock 1998; Jura 2006) and may even produce the observed X-ray emission at 1 keV. Furthermore, Debes & Sigurdsson (2002) suggest that if the surviving planet system becomes unstable after the AGB phase, the entire system becomes dynamically young; i.e., frequent collisions and encounters can occur among surviving planets and comets, leading to a period of enhanced “late bombardment.” It is likely that the kilometer-size objects surviving around the Helix central star are experiencing similar perturbations and producing fine dust in the system. The Poynting-Robertson (P-R) lifetime is $(3\text{--}50) \times 10^6$ yr for $\sim 100 \mu\text{m}$ grains located at 35 and 150 AU, while the collisional lifetime is $(0.1\text{--}1) \times 10^6$ yr. Note that these timescales are much longer than the kinematic age of the nebula (2.8×10^4 yr; Napiwotzki 1999) and a typical timescale in the post-AGB evolution ($\sim 4 \times 10^4$ yr for a $0.565 M_{\odot}$ white dwarf; Schönberner 1983). Assuming an average dust lifetime of 1×10^6 yr, the dust production rate is $2.5 \times 10^{13} \text{ g s}^{-1}$. This rate is only a lower limit since the dust production is not in equilibrium, but it is $\sim 10^5$ times the dust production rate observed from comet Hale-Bopp, consistent with the hypothesis of an enhanced late bombardment in the post-main-sequence evolution.

The total observed dust mass, $\sim 0.13 M_{\oplus}$, is equivalent to 20 asteroidal objects with a radius of ~ 1200 km. While the dust cloud around the white dwarf G29-38 may arise from tidal disruption of Pluto-sized objects (Jura 2003), this cannot be the case for the disk in WD 2226–210 because the tidal disruption zone is much closer to the central star, ~ 0.003 AU (Jura 2003, eq. [4]). It is thus unlikely that the debris disk is produced by tidal breaking of large asteroidal objects but rather by enhanced collisions among the surviving Kuiper Belt-like and/or cometary objects.

The inner radius of a P-R drag-dominated disk, in general, should be very close to the star, up to the dust sublimation radius (~ 0.1 AU in the case of the Helix central star) if there is no planet-size or substellar object inside the disk to stop the dust grains from spiraling inward. The inner hole ($r \lesssim 35$ AU)

derived from our SED model is likely caused by the dynamical perturbation of unseen planets or substellar objects inside the hole, which can trap the migrating dust or scatter the dust outward (Meyer et al. 2007). Alternatively, the inner hole may also be explained by ice sublimation if the grains are icy (Jura et al. 1998), a process that will occur at a dust temperature of ~ 150 K, corresponding to ~ 30 AU.

If the Helix central star had a close binary in the main-sequence phase, a binary merger event could produce an accretion disk around the remaining white dwarf. The physical structure of the disk would be highly dependent on the properties of the original binary system; however, the fact that there is no near-infrared excess suggests that the inner part of the optically thick accretion disk would have to dissipate in a short period of time after the binary merged. It is hard to explain why the dust is so far away from the white dwarf if it was the remnant disk due to close binary evolution. Alternatively, if the companion was in an intermediate orbit and avoided spiraling into the primary during the evolution, the binary con-

figuration is efficient at trapping the dust from the mass loss of the primary to form a stable circumbinary disk in the post-AGB phase (van Winckel 2003; de Ruiter et al. 2006), inducing the presence of the dusty disk we detected. However, any of the micron-size dust generated in the AGB phase should be blown out by the strong radiation in the early white dwarf evolution. The fact that we do see dust around the Helix central star favors the debris disk scenario. Future high spatial resolution infrared imaging is needed to further constrain the geometry of the emitting region.

This work is based on observations made with the *Spitzer Space Telescope*, which is operated by the Jet Propulsion Laboratory, California Institute of Technology, under NASA contract 1407. Code for calculating optical properties of grains at large size parameters kindly provided by Viktor Zubko and Karl Misselt. Support for this work was provided by NASA through contract 1255094, issued by JPL/Caltech. T. R. was supported by the BMBF/DESY under grant 05 AC6VTB.

REFERENCES

- Becklin, E. E., Farihi, J., Jura, M., Song, I., Weinberger, A. J., & Zuckerman, B. 2005, *ApJ*, 632, L119
- Bohlin, R. C., Harrington, J. P., & Stecher, T. P. 1982, *ApJ*, 252, 635
- Ciardullo, R., Bond, H. E., Sipior, M. S., Fullton, L. K., Zhang, C.-Y., & Schaefer, K. G. 1999, *AJ*, 118, 488
- Debes, J. H., & Sigurdsson, S. 2002, *ApJ*, 572, 556
- de Ruiter, S., van Winckel, H., Maas, T., Lloyd Evans, T., Waters, L. B. F. M., & Dejonghe, H. 2006, *A&A*, 448, 641
- Dohnanyi, J. W. 1969, *J. Geophys. Res.*, 74, 2531
- Duncan, M. J., & Lissauer, J. J. 1998, *Icarus*, 134, 303
- Fazio, G. G., et al. 2004, *ApJS*, 154, 10
- Gordon, K. D., et al. 2005, *PASP*, 117, 503
- Gruendl, R. A., Chu, Y.-H., O'Dwyer, I. J., & Guerrero, M. A. 2001, *AJ*, 122, 308
- Guerrero, M. A., Chu, Y.-H., Gruendl, R. A., Williams, R. M., & Kaler, J. B. 2001, *ApJ*, 553, L55
- Harris, H. C., et al. 2007, *AJ*, 133, 631
- Higdon, S. J. U., et al. 2004, *PASP*, 116, 975
- Hora, J. L., Latter, W. B., Smith, H. A., & Marengo, M. 2006, *ApJ*, 652, 426
- Houck, J. R., et al. 2004, *ApJS*, 154, 18
- Jura, M. 2003, *ApJ*, 584, L91
- . 2006, *ApJ*, 653, 613
- Jura, M., Malkan, M., White, R., Telesco, C., Pina, R., & Fisher, R. S. 1998, *ApJ*, 505, 897
- Kilic, M., von Hippel, T., Leggett, S. K., & Winget, D. E. 2005, *ApJ*, 632, L115
- Laor, A., & Draine, B. T. 1993, *ApJ*, 402, 441
- Leahy, D. A., Zhang, C. Y., & Kwok, S. 1994, *ApJ*, 422, 205
- Leene, A., & Pottasch, S. R. 1987, *A&A*, 173, 145
- Meyer, M. R., Backman, D. E., Weinberger, A. J., & Wyatt, M. C. 2007, in *Protostars and Planets V*, ed. B. Reipurth, D. Jewitt, & K. Keil (Tucson: Univ. Arizona Press), 573
- Napiwotzki, R. 1999, *A&A*, 350, 101
- O'Dell, C. R., McCullough, P. R., & Meixner, M. 2004, *AJ*, 128, 2339
- Parriott, J., & Alcock, C. 1998, *ApJ*, 501, 357
- Rauch, T., & Deetjen, J. L. 2003, in *ASP Conf. Ser. 288, Workshop on Stellar Atmosphere Modeling*, ed. I. Hubeny, D. Mihalas, & K. Werner (San Francisco: ASP), 103
- Reach, W. T., Kuchner, M. J., von Hippel, T., Burrows, A., Mullally, F., Kilic, M., & Winget, D. E. 2005, *ApJ*, 635, L161
- Rieke, G. H., et al. 2004, *ApJS*, 154, 25
- Sackmann, I.-J., Boothroyd, A. I., & Kraemer, K. E. 1993, *ApJ*, 418, 457
- Schöenberger, D. 1983, *ApJ*, 272, 708
- Siess, L., & Livio, M. 1999a, *MNRAS*, 304, 925
- . 1999b, *MNRAS*, 308, 1133
- Stern, S. A., Shull, J. M., & Brandt, J. C. 1990, *Nature*, 345, 305
- Tanaka, H., Inaba, S., & Nakazawa, K. 1996, *Icarus*, 123, 450
- Traulsen, I., Hoffmann, A. I. D., Rauch, T., Werner, K., Dreizler, S., & Kruk, J. W. 2005, in *ASP Conf. Ser. 334, 14th European Workshop on White Dwarfs*, ed. D. Koester & S. Moehler (San Francisco: ASP), 325
- van Winckel, H. 2003, *ARA&A*, 41, 391
- Werner, K., Dreizler, S., Deetjen, J. L., Nagel, T., Rauch, T., & Schuh, S. L. 2003, in *ASP Conf. Ser. 288, Workshop on Stellar Atmosphere Modeling*, ed. I. Hubeny, D. Mihalas, & K. Werner (San Francisco: ASP), 31
- Young, K., Cox, P., Huggins, P. J., Forveille, T., & Bachiller, R. 1999, *ApJ*, 522, 387
- Zuckerman, B., & Becklin, E. E. 1987, *Nature*, 330, 138

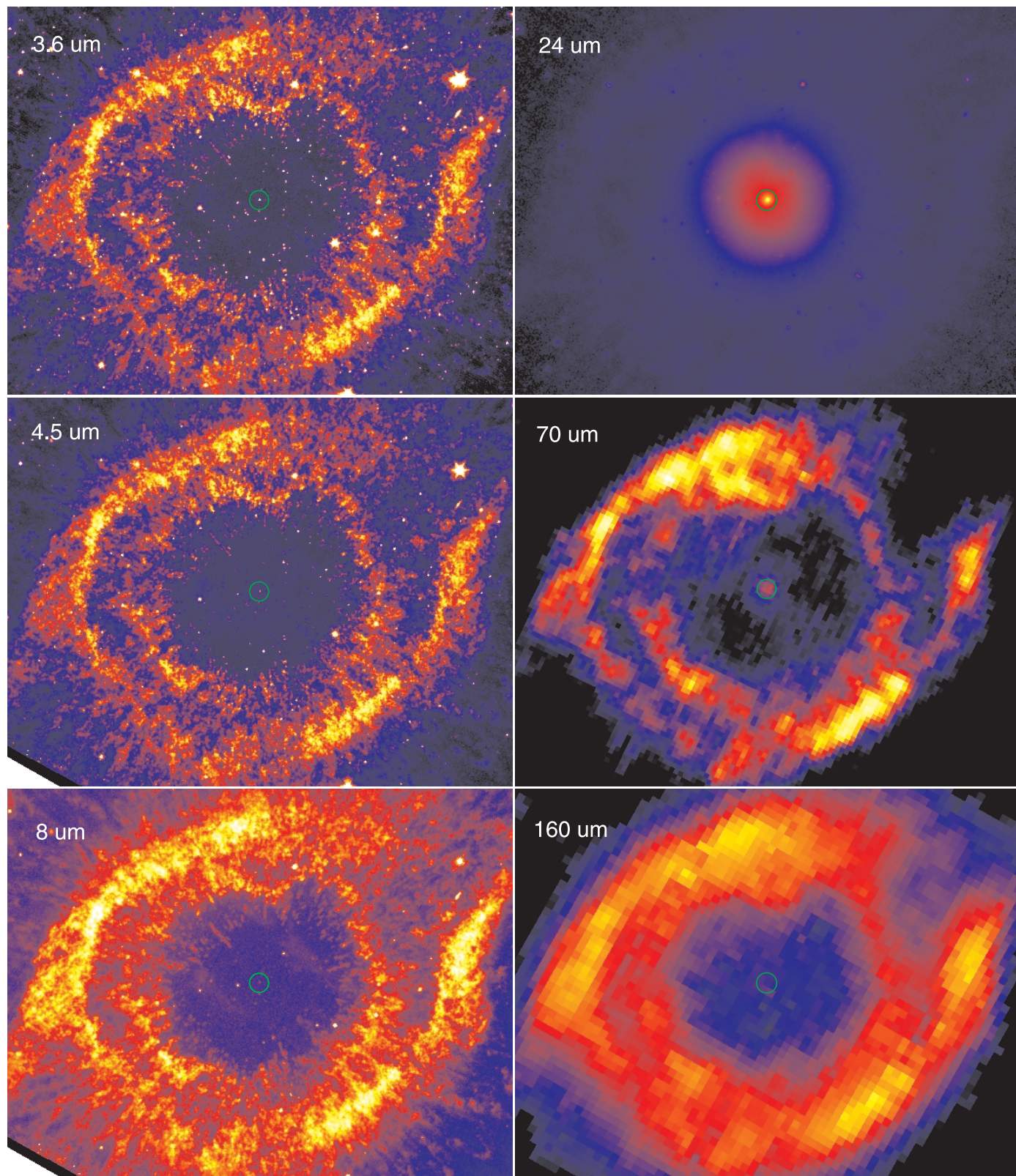


PLATE 1

FIG. 1.—*Spitzer* images of the Helix Nebula. Each panel is displayed in a false-color logarithmic scale with brightness and contrast adjusted for best presentation and oriented as north up and east toward the left with a field of view of $15.4' \times 12.5'$.